THE PENNSYLVANIA STATE UNIVERSITY
SCHREYER HONORS COLLEGE

DEPARTMENT OF MATERIALS SCIENCE AND ENGINEERING

Cold Sintering of Zinc Oxide Polyimide Composites with Internally Tunable Electrical Properties via Polymer Crosslinking

ADAM VETSER
SUMMER 2023

A thesis
submitted in partial fulfillment
of the requirements
for a baccalaureate degree in Materials Science and Engineering
with honors in Materials Science Engineering

Reviewed and approved* by the following:

Clive A. Randall
Distinguished Professor of Materials Science and Engineering
Thesis Supervisor

Robert Allen Kimel
Associated Teaching Professor of Materials Science and Engineering
Honors Adviser

* Electronic approvals are on file.

ABSTRACT

This thesis investigates the fabrication, microstructure, crosslinking, and bulk electrical properties of a ZnO polyimide composite. Single step processing for ceramic-polymer composites has been unattainable due to the gap between ceramic and polymer processing temperatures using traditional sintering methods >1000°C. The cold sintering process (CSP) of ZnO occurs at 250°C, allowing for the integration of polymeric materials below their crosslinking temperature without degradation. Five methods of dispersing the polyimide in ZnO were investigated with the goal of obtaining a homogenous polymer dispersion and high density. Integration of the polyimide to ZnO through the creation of a polymer dispersion in an organic solvent yielded a 94.7% relatively dense composite. Electrical impedance spectroscopy (EIS) was used to characterize the bulk electrical properties of the composite before and after crosslinking at 380°C. Resistivity was shown to decrease by an order of magnitude while the activation energy for electron conduction increased after crosslinking. A mechanism for polyimide crosslinking was proposed using Fourier-transform infrared spectroscopy (FTIR) to explain the observed electrical trends. Ceramic-polymer composites offer applications including semiconductors, piezoelectrics, varistors, and solar cells. The development of single step ceramic-polymer composite processing could allow for devices with internally tunable electrical properties as a function of applied heat.

TABLE OF CONTENTS

LIST OF FIGURES

LIST OF TABLES

ACKNOWLEDGEMENTS

Thank you to Zane Grady, Dr. Clive Randall, Arnaud Ndayishimiye, and all members of the Materials Research Institute and Millennium Science Complex who helped support me in my undergraduate research. Thank you to my peers both at PSU and beyond who have shaped my college experience and were there to support me personally so that I could succeed academically. I know you will thrive wherever your next chapter takes you.

I am not here without the unconditional love of my mom, dad, sister, grandparents, and the rest of my family. Thank you for bolstering me at my lowest moments and celebrating with me at my highest moments. To the wisest and most knowledgeable man I've known, my grandpa or guppy, you have and will continue to inspire the man I am. Thank you for instilling a love of learning in me.

Chapter 1

Introduction

Traditional sintering of ceramic materials occurs in excess of 1000 °C and can take over 10 hours to achieve a desirable 95% relative density [**Error! Reference source not found.**]. This places a high energy demand on the manufacturing of ceramic composites and makes their densification incompatible with low temperature materials like polymers. Ceramic-polymer composites offer a unique set of properties making them desirable for mechanical, thermal, optical, and especially electronic applications where they are used in semiconductors, piezoelectrics, varistors, and solar cells.

The cold sintering process (CSP) uses low sintering temperatures, offering the opportunity to process both ceramics and polymers in a single step without polymer degradation. Cold sintering involves the introduction of transient solvent to aid in the dissolution-precipitation process of densification. This thesis explores a ZnO polyimide composite produced via cold sintering with an acetic acid transient solvent. A uniaxial load is applied at 250°C to yield a highly dense ceramic. Ion mass transport through the introduced liquid transient phase following chemical potential gradients reorders the structure to reduce free surface energy [1]. Through a thermodynamic driving force, porosity is reduced, and the ceramic is densified [1].

Ceramic densification occurs below the polyimide's crosslinking temperature. By raising the polymer above this crosslinking temperature, adjacent polymer chains undergo a non-reversible chemical reaction to form covalent bonds [3]. Processing below the crosslinking temperature affords the novel opportunity to internally tune the bonding chemistry of the

polymer post-processing. It was hypothesized that forming these polymer crosslinks would impede the flow of electrons due to polymers' poor electrical conduction, thereby irreversibly altering the bulk electrical properties of the composite (Figure 1.1).

Figure 1.1 Idealized Composite Microstructure

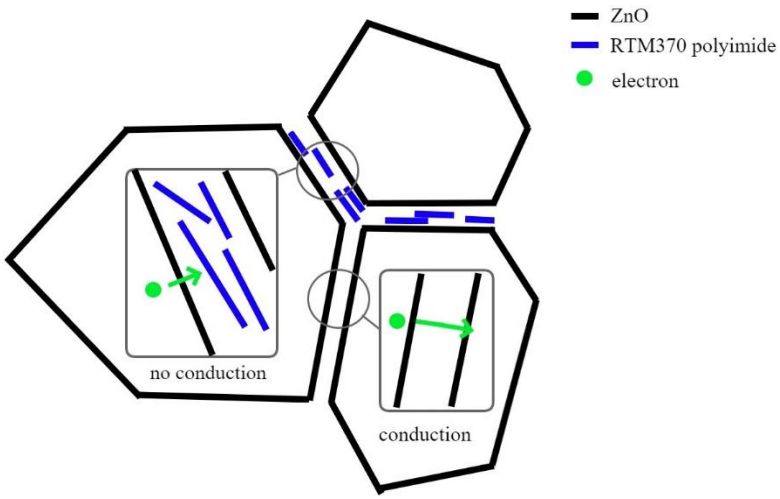

1.1 Motivations

Cold sintering is a relatively new discovery in the field of ceramics, only first being widely investigated in 2016 [1]. Given this, its applications on specific systems like ceramic-polymer composites still have room for exploration. The ability to process ceramic in a low temperature regime opened the opportunity for single-step manufacturing with low temperature materials. The literature lacks exploration of the ability to internally manipulate composite phases as opposed to chemical manipulation prior to combining multiple materials, which is normally how composites achieve desirable properties. The ZnO-polyimide system investigated in this thesis would serve as proof of concept for ceramic-polymer composites with internally tunable electrical properties as a function of applied heat. Though single single-step manufacturing of

ceramic-polymer composites is introduced in the literature, there is no standard methodology for polymer dispersion. It was not known how the ZnO, polyimide, and CSP transient solvent would interact with one another prior to and during CSP. In order to successfully investigate internal polymer crosslinking, it was first necessary to understand how mixing the polyimide, ZnO, and acetic acid transient solvent for the CSP impacted polymer dispersion and the relative density of the bulk composite.

The polymer investigated is the resin transfer molded polyimide RTM370 obtained from NASA Glenn Research Center. Ceramic-polymer composites using this chemistry have never been created. This serves both as a test of the capabilities of the CSP to succeed on novel materials as well as an opportunity to characterize the electrical properties of a unique polyimide.

1.2 Objectives

The objective of this investigation is the successful fabrication of a 95% dense homogenously dispersed ZnO-polyimide composite via cold sintering. The identification of a homogenous polymer dispersion methodology can be used as a reference to the cold sintering of similar systems. The next objective would be to show that the polyimide can be crosslinked inside of the composite. This will be used to determine the impact of a crosslinked polyimide microstructure on the bulk electrical properties of the composite. This characterization would help identify applications that can make use of internally tunable ceramic polymer composites.

1.3 Broader Impacts

Cold sintering can have a broader impact on climate change by reducing the carbon footprint of ceramic-polymer composite manufacturing. Brick and cement production alone demonstrates the need for a low temperature processing method for ceramic densification. 1.23 trillion bricks are produced annually, which are responsible for 8% of annual carbon dioxide emissions or approximately the annual emissions of the entire airline industry [4,5]. The main manufacturing challenge with producing composites is the opposing temperature regimes of ceramics and polymers. Traditionally fabricating composites has a high energy cost associated with the continuous heating, maintaining, and cooling of furnaces between these temperature regimes. Using the CSP decreases energy demand by rolling production into a single low temperature step and eliminating the need to toggle between temperatures.

This single step manufacturing can have a broader impact when considering high-volume manufacturing, renewable energy applications, and recyclability. The CSP can help reduce emissions from the production of circuitry components such as varistors from ceramic semiconductor materials. These components are often produced in bulk, making the impact of even a minor energy savings significant during the manufacturing process [6]. Ceramic-polymer composites also play a direct role in the production of renewable energy via solar cell applications [7]. Components manufactured via the CSP are more reformable and reprocessable compared to traditionally produced compsites, contributing to the creation of a circular economy [8]. This way, the CSP has an opportunity to impact climate change on three levels of emissions.

Chapter 2
Background

The system explored in this thesis is zinc oxide (ZnO) and the polyimide RTM370 with a 2 M acetic acid transient solvent. The background will cover relevant literature and information for each material in the system, the thermodynamic and kinetic mechanisms involved with the CSP at the ZnO and acetic acid interface, the characterization methods used to gather data in the experimental procedure, and relevant applications.

2.1 Materials

2.1.1 RTM370 Polyimide

RTM370 is the polyimide used in the created composite and was obtained from the NASA Glenn Research Center. A polyimide is a class of polymer containing the imide functional group. “370” refers to the reported 370°C glass transition temperature, which was found to correlate to the onset of irreversible crosslinking [9]. Crosslinking refers to the covalent bonding of adjacent polymer chains at the 370°C threshold temperature. Below this threshold, chains are only weakly bonded through Van der Waals interactions. RTM refers to “resin transfer molding,” a low-cost forming method typically used in aerospace applications. The polyimide’s low-melt viscosity and high glass transition temperature makes it of value in this investigation. At the CSP processing temperature of 250°C RTM370 melts but does not yet undergo a glass transition, as there is a wide gap between 250°C and the glass transition temperature of 370°C. This ensures no polymer chemical transitions occur during the ceramic

sintering. Polyimide crosslinking can then be explored as an isolated process that occurs inside the composite post-densification. The crosslinked polyimide is of interest for the general application of ceramic-polymer composites for its high temperature capabilities and desirable mechanical properties.

The polyimide is comprised of three independent oligomers 2,3,3',4'-biphenyltetracarboxylic dianhydride (a-BPDA), 3,4'-oxyaniline (3,4'-ODA), and 4-phenylethynylphthalic anhydride (PEPA) (Figure 2.1 [9]) which are melted and imidized to synthesize resins using a solvent-free process.

Figure 2.1 Oligomers Used in the Production of RTM370

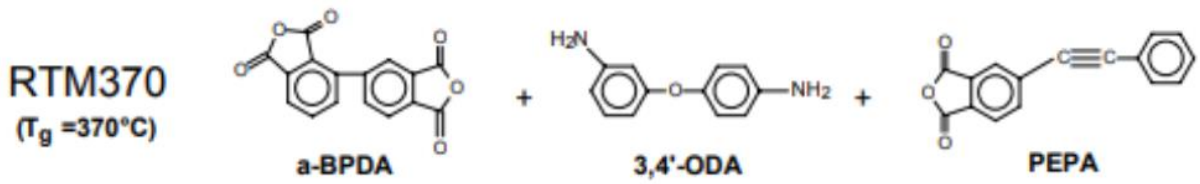

polymerization occurs through reactions of the diamine, 3,4'-ODA, where the reactive amines bond with the anhydride groups on the a-BPDA and PEPA to form an imide functional group and water as a biproduct, hence the classification as a polyimide (Figure 2.2 [9]). The free anhydride available on the a-BDPA allows for extension of the polymer chain while PEPA acts as an endcap to the chain. FTIR analysis will be used to propose a crosslinking mechanism and structure for RTM370.

Figure 2.2 RTM370 Polyimide Functional Groups and Imidization

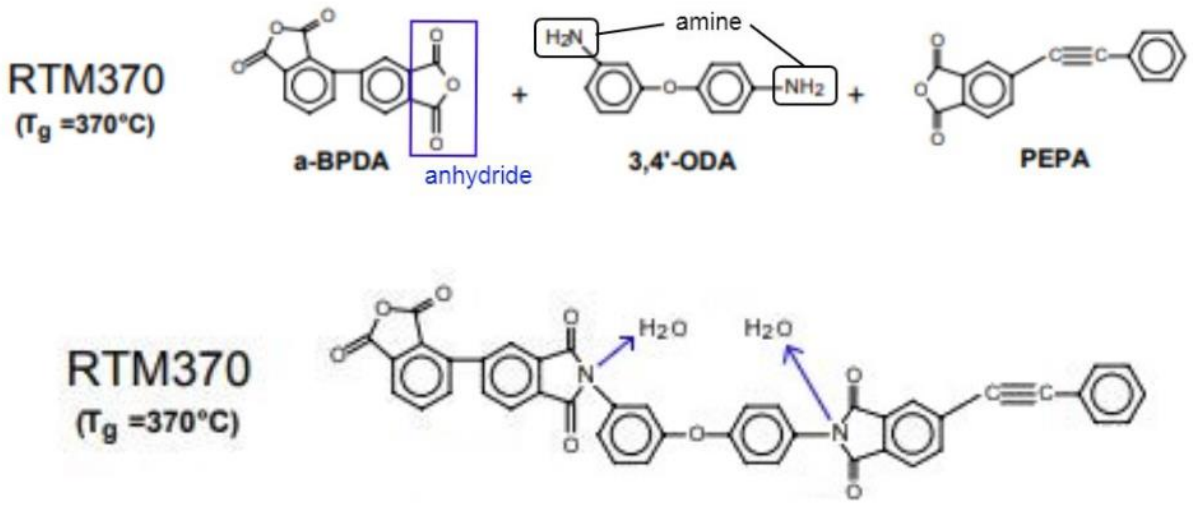

2.1.2 ZnO

Understanding the surface crystal chemistry of ZnO is key for understanding the CSP. In this investigation, ZnO has a wurtzite crystal structure with a 1.99 Å Zn-O bond length [10]. Each Zn^{2+} and O^{2-} atom is 4 coordinated, meaning they form 4 bonds each in a tetrahedral arrangement (Figure 2.3) [11]. At the termination of the ZnO crystal, Zn^{2+} and O^{2-} atoms have fewer than the 4 bonds that their coordination suggests, most commonly 3 bonds leaving either a Zn^{2+} or O^{2-} dangling bond [11]. Given the ionic nature of the crystal bonding, these dangling bonds have an electrostatic charge preference, or zeta potential. Zn^{2+} has a 2^+ charge, therefore its dangling bond has a negative zeta potential while O^{2-} has a charge of 2^-, so its dangling bonds have a positive zeta potential [11]. As a result, planes exhibit specific polarities because of their dangling bonds [12]. The (001) face, or top face demonstrated in Figure 2.4, has dangling bonds from the positively charged Zn^{2+} ions and therefore attracts negative species. The opposite $(00\bar{1})$ face has dangling bonds from the negatively charged O^{2-} ions and therefore attracts positive

species. Figure 2.5 demonstrates this phenomenon on an atomic scale in the crystal. The intersection of ZnO surface crystal chemistry and the aqueous chemistry of the acetic acid transient solvent help to develop an understanding of the mechanism of the CSP.

Figure 2.3 Dangling Bonds of the (00$\bar{1}$) and (001) ZnO Planes

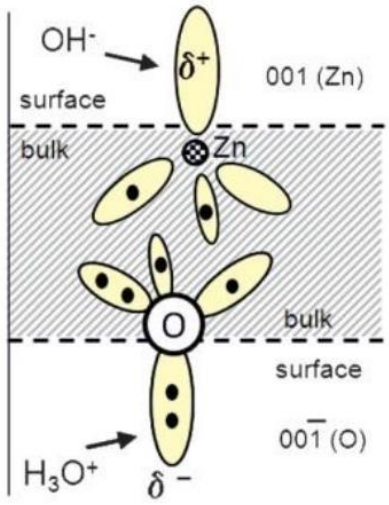

Figure 2.4 Polarity of ZnO Planes

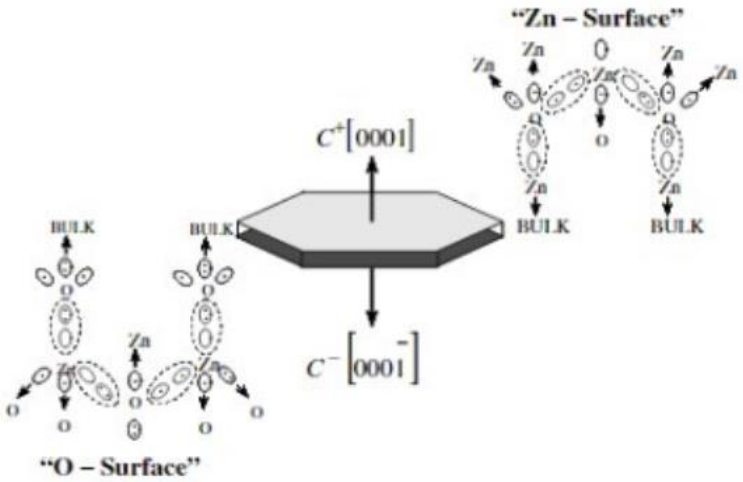

Figure 2.5 ZnO Wurtzite Crystal Structure

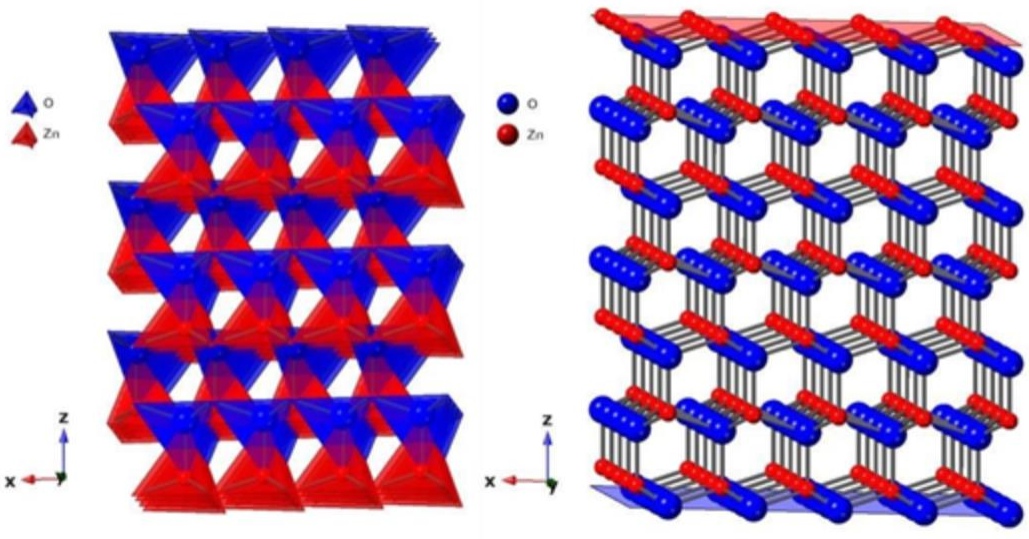

2.2 Processing

Traditional sintering occurs in excess of 1000 °C, making it incompatible with low temperature regime materials like polymers. The cold sintering process (CSP) allows for ceramic densification at temperatures below 300°C with the addition of uniaxial pressure and a transient solvent phase. The solvent is referred to as transient because cold sintering operates as an open system, meaning that, after acting as a transport phase for sintering, the solvent is evaporated out. The sintering process occurs through three steps called etching, dissolution-rearrangement, and dissolution-precipitation [13]. During etching, the transient solvent acetic acid acts to wet the ceramic particles and dissolves the surface ZnO. Following etching is the dissolution-rearrangement stage where the dissolved Zn^{2+} and O^{2-} ions are transported to different low-density regions of the structure like pores. Finally, one proposed mechanism states that the dissolved ions in the transient solvent are precipitated on the crystal surface to minimize the free

surface energy of the system. This yields a densified or sintered structure. The etching step will be explored in detail to understand the factors that lead to the dissolution-precipitation mechanism of the CSP.

Ion mass transport as a part of the dissolution-rearrangement stage arises from thermodynamic and kinetic interactions between the surface chemistry of ZnO and the transient solvent acetic acid. The species in the acetic acid transient solvent dissociate into charged ions which interact with the ZnO surface of appropriate zeta potential. Speciation, or the formation of more thermodynamically favorable chemical species, occurs which breaks the ionic bonds between Zn^{2+} and O^{2-} to etch the crystal. The chemistry of etching for this thesis's ZnO acetic acid system will be specified by reviewing the steps of acetic acid dissociation and speciation at the crystal surface.

The 2 M acetic acid solution used as the ZnO solvent contains water and acetic acid, CH_3COOH. The water dissociates to yield positively charged protons, H^+, and negatively charged hydroxide, OH^-, and the acetic acid dissociates to yield negatively charged acetate, CH_3COO^-, and positively charged protons, H^+ [14]. The H^+ protons will then form H_3O^+ after dissociation.

Figure 2.6 Dissociation Reactions of Species in Acetic Acid Transient Solvent

$$H_2O_{(aq)} \rightarrow H^+_{(aq)} + OH^-_{(aq)}$$

$$CH_3COOH_{(aq)} \rightarrow H^+_{(aq)} + CH_3COO^-_{(aq)}$$

The dominant etching mechanism for Zn^{2+} dangling bonds is speciation with acetate ion to form zinc acetate, $ZnC_4H_8O_4$ (Figure 2.7). The dominant etching mechanism for O^{2-} dangling bonds is

speciation with two H^+ ions to form water, H_2O. The supplemental animation submitted with this thesis demonstrates the etching process for various faces of the ZnO crystal [15].

Figure 2.7 Zinc Ion Etching via Acetate Speciation

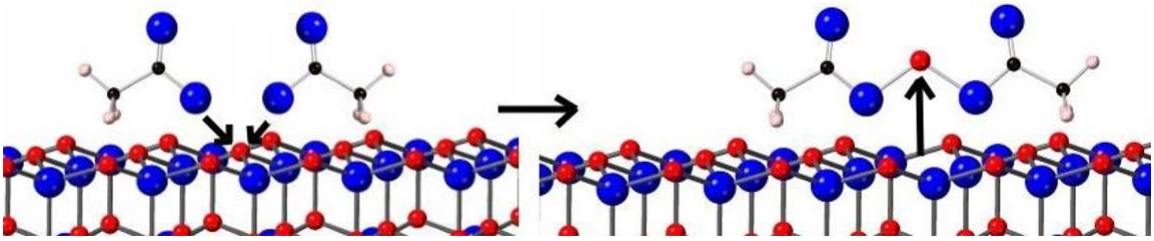

The rate of etching is dependent upon acetic acid dissociation rates, the kinetics of ion migration to the ZnO surface, and the proportions of dangling bonds present on a given crystal face. Acetic acid dissociation rates are pH and temperature dependent, where higher pH transient solvents will contain higher concentrations of H^+ ions and the dissociation rate of water dominates as temperature increases. The kinetics of ion migration are dependent on steric considerations and therefore the hydrodynamic radius of the ions. Since H^+ ions are smaller, they diffuse faster to the crystal surface and overlap less with the ZnO. Dangling bond proportions differ by face as a function of bulk crystal chemistry, so some surfaces inherently have faster etching rates than others. These aqueous and crystal chemistry considerations impact etching rate and therefore how a cold sintered structure is formed.

The etching mechanism outlined above is immediately proceeded by ion mass transport of the etched species, creating a denser sintered structure.

2.3 Characterization

Electronic Impedance Spectroscopy (EIS), Fourier-Transform Infrared Spectroscopy (FTIR), Scanning Electron Microscopy (SEM), and Energy Dispersive X-Ray Spectroscopy (EDS) were used to analyze the composite samples.

2.3.1 Impedance Spectroscopy

EIS was the main electrical characterization method used for analyzing the effect of crosslinking the polymer inside the bulk composite. Impedance spectroscopy is a measure of an material's electrical response to an applied sinusoidal voltage as a function of frequency, allowing for the distinguishing of bulk and grain boundary effects [16]. The results are then quantified and analyzed through the construction of an equivalent circuit, which is an idealization of the electrochemistry of the sample's microstructure. This thesis used a ZARC component (Figure 2.8 [17]) consisting of a resistor in series with a resistor and capacitor in parallel.

Figure 2.8 ZARC Equivalent Circuit Model for EIS

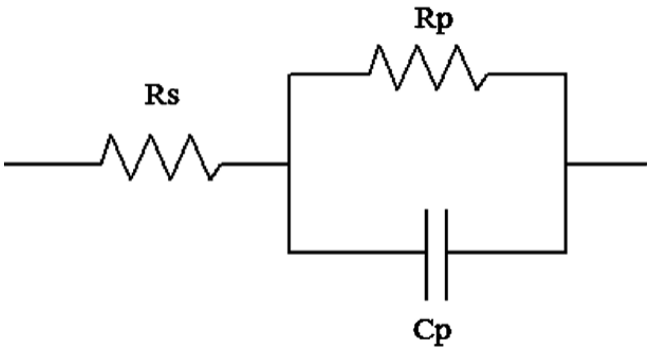

Different frequency dependent properties can now be measured including permittivity (ε^*) or the material's ability to store electrical energy, dielectric loss ($\tan \delta$) or the measure of

electric dissipation, and impedance (Z*) or resistance to the flow of electricity. Different formalisms which emphasize different frequency ranges of impedance are also possible including admittance (Y*) and modulus (M*). Figure 2.9 demonstrates the equations for calculating these values [18].

Figure 2.9 Impedance Equations

$$\varepsilon^* = \varepsilon' - j\varepsilon''$$

$$M^* = M' + jM'' = 1/\varepsilon^*$$

$$Z^* = Z' - jZ'' = 1/j\omega C_0 \varepsilon^*$$

$$Y^* = Y' + jY'' = j\omega C_0 \varepsilon^*$$

$$C_0 = \frac{\varepsilon_0 A_c}{L}$$

ω refers to the angular frequency, C_0 the geometric capacitance where A_c and L are electrode area and separation distance in cm^2 and cm respectively, and $j = \sqrt{-1}$. The presence of the *j* term allows for the plotting of impedance on a complex plane that demonstrates frequency dependence known as a Nyquist plot (Figure 2.10 [16]).

Figure 2.10 EIS on complex plane for YIG ceramic

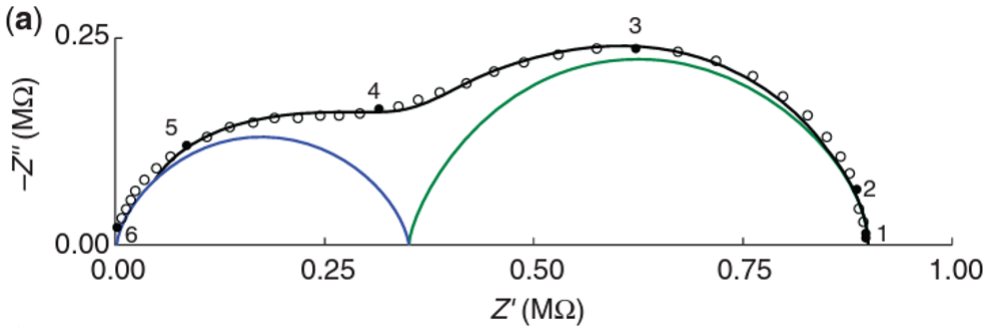

The data is fitted with semicircles to determine the number of responses. The semi-circle's intersection with the x-axis is an indication of resistivity. When the shape of the semi-circle is uniform, the frequency in which electrons jump is homogenous [16].

2.3.2 FTIR

FTIR was the main chemical characterization method used for analyzing the crosslinking of the RTM370 polyimide. In FTIR, a sample is exposed to high energy infrared (IR) radiation. The bonds of the sample molecules absorb some of the IR radiation, and a unique absorption peak is formed corresponding to the vibrational frequency of that bond. In this way, a "fingerprint" of the sample's bonding structures can be generated [19].

2.3.3 SEM/EDS

SEM and EDS were the main characterization methods used to analyze the microstructure of sintered samples.

SEM functions through the generation of an electron beam which is accelerated towards a sample. To be observed, the surface of a sample must be electrically conductive, so non-conductive samples are first coated with materials such as iridium. Upon impact on a sample surface, the energy of the incident beam incites electron promotion in the sample surface, resulting in the emission of secondary electrons. These electrons are then collected and turned into an electrical signal by fluorescent detector materials, the locations of which are determined via correlating the scanning position of the incident beam. Backscattering also occurs, where

incident electrons reflect off the sample surface and are then detected. SEM has a resolution on the scale of single micrometers [20].

EDS functions through reading photons emitted from ionized atoms on the surface of the sample as secondary electrons are being generated for imaging. The energy of these photons is a quantized value in the X-ray range, and therefore are characteristic of the atom they were emitted from. The collection of these characteristic photons via a detector allows for the creation of an elemental profile of the surface of the sample [20].

2.4 Applications

Varistors are circuitry components used primarily to protect electronic devices from overvoltage, usually from electric impulses caused by lightning or switching surges. Studies of households in the United States show that impulses with destructive capabilities occur multiple times daily, indicating a need for overflow protection to prevent considerable infrastructure damage. ZnO varistors were introduced in the 1970s and are widely used today for up to 1000 V protection [21].

The fabrication of ZnO composites opens the opportunity to develop varistors with novel electrical properties. Varistor conduction is highly dependent upon the microstructure of ZnO. With the polyimide composite investigated in this thesis electrical conduction becomes internally tunable as a function of heat, which was previously not possible. Reaching a threshold temperature would induce polyimide crosslinking, impacting electrical conduction and therefore varistor performance. The impact of crosslinking on conduction will be investigated in this thesis to evaluate if there is any utility in this mechanism.

Introduction of a polymer phase could also impact the mechanical properties of the ZnO. Varistors with higher performing physical properties could be used for applications where previous metal oxide varistors mechanically failed.

Chapter 3

Experimental Procedure

3.1 Materials

Precursor materials include < 5 μm zinc oxide (ZnO) from Sigma-Aldrich and crystallized RTM370 polyimide was obtained from Dr. Kathy Chuang at the NASA Glenn Research Center. 2 M acetic acid was diluted from glacial acetic acid from VWR Brand, and the organic solvent N-Methyl-2-pyrrolidone (NMP) was obtained from Sigma Aldrich. Details for all precursor materials are provided in Table 3.1

Table 3.1 Precursor Materials

Chemical	Purity	Manufacturer
ZnO	99.9%	Sigma-Aldrich
RTM370	-	NASA Glenn Research Center
Glacial acetic acid	99.7%	VWR Brand
NMP	≥99.9%	Sigma-Aldrich

3.2 Mixing Methodologies

Five mixing methodologies were tested to determine which one yields a high density and homogenous ZnO-polyimide composite pellet. Each mixing method and the preparation for pure ZnO sintering is detailed in this section.

3.2.1 Pure ZnO

0.5 g of powder was created by adding 26 µl of 2 M acetic acid via micropipet or 5 wt% to 0.5 g ZnO in a mortar and pestle. The components were mixed until the mixture behaved like a dry powder as opposed to a slurry.

3.2.2 Dry Hand

The dry hand method involved no organic solvent aid for polymer dispersion. 0.5 g of powder was created with 5 wt% or 17.7 vol% polyimide and 95 wt% or 82.3 vol% ZnO. 0.025 g of polyimide was added to 0.475 g of ZnO in a mortar under a fume hood. 26 µl of 2 M acetic acid or 5 wt% was added as the transient solvent. The components were mixed.

3.2.3 Wet Hand

The dry hand method was repeated but 0.75 g powder was created. 0.7125 g ZnO and 0.0375 g polyimide were mixed with 37.5 µl of NMP or 5 wt% was added to aid as an organic solvent to disperse the polyimide. The components were mixed.

3.3.3 Cryomill

Preparation of 3 g of ZnO polyimide powder was needed to reach the minimum for the cryomilling equipment. 0.075 g of polyimide was added to 2.925 g of ZnO and loaded into a Retsch CryoMill cooled via liquid nitrogen to -196 °C. The cryomill was run for 3 2-minute 25 Hz cycles in a stainless-steel holder with a 15 mL stainless steel media ball [22]. 2.816 g of usable powder was obtained for the cold sintering of composite pellets. 35.7 µl of 2 M acetic acid was added via micropipette to a mortar and pestle containing 0.75 g of the mixed ZnO polyimide powder. The components were mixed.

3.2.4 1-Step Polysol

A solution comprised of a polymer dispersed in an organic solvent, referred to as a polysol in this thesis, was prepared prior to integration with ZnO powder. A 30 wt% polymer solution was prepared. 10 mL NMP was measured added it a 20 mL vial. The vial was heating below 80°C to prevent NMP evaporation while stirring with a stir bar on a hot plate located in a fume hood. 4.41 g polyimide was slowly added, ensuring that the previous polymer was dissolved before adding new polymer. If the polysol was stored for more than 1 hour before use in the CSP, heating to 90°C was necessary to uncongeal the solution. The polysol was transferred immediately after heating, as the solution increased in viscosity as it cooled and was unable to be transferred via micropipette. 33.8 µl polysol and 35.7 µl acetic acid was added via micropipette to a mortar and pestle containing 0.675 g of ZnO. The components were mixed.

3.2.5 2-Step Polysol

The 2-step polysol method involved creating a polysol suspension, adding ZnO, and burning off the excess NMP organic solvent prior to use for the CSP. 3.952 g ZnO and 0.048 g of RTM370 polyimide were added to 37 mL of NMP. The solution was set on a 90°C hot plate under a fume hood for approximately 30 minutes or until the NMP completely evaporated. Powder yield was 97.8%. 35.7 µl acetic acid was added via micropipette to a mortar and pestle containing 0.75 g of the mixed ZnO polyimide powder. The components were mixed.

3.3 Synthesis Procedure

The mixed and dispersed powder was loaded into a steel die with a thermocouple jacket attached to a temperature controller. The temperature control was set to 250°C and the die was placed in a uniaxial Carver press with 340 MPa or 10,000 lbs. of pressure applied. The setup was monitored for the first 5 minutes to ensure there is no pressure loss. The pressure was released, and the die was cooled after 1 hour of sintering. The Archimedes density method with ethanol was used to calculate the relative density of the sintered pellet. Sintered pellets were stored in an 80°C vacuum oven.

3.4 Chemical Characterization

3.4.1 Crosslinking

In order to determine a procedure for crosslinking the polymer inside the composite pellet, polymer crosslinking was first corroborated externally. Samples of uncrosslinked polyimide were placed in stainless-steel cylinders with aluminum foil bottoms in alumina holders as secondary containment (Figure 3.1). Three samples were placed into box furnaces for 5, 30, and 60 minutes respectively at 380°C. This temperature was selected to ensure the 370°C glass transition temperature was reached [9]. A small piece of polymer was removed for FTIR analysis.

Figure 3.1 External Polyimide Crosslinking Experimental Setup

3.4.2 FTIR

FTIR analysis using a Bruker Vertex V80v was performed on uncrosslinked polyimide powder, and the three samples of heat-treated polyimide [23]. Results were compared to chemically confirm crosslinking and developed a proposed crosslinking mechanism via the Infrared and Raman Characteristic Group Frequencies guide by George Socrates.

3.5 Physical Characterization

Samples were broken in half for SEM/EDS analysis and coated with 5 nm of conductive iridium. A Verios NanoSEM field-emission SEM was used with a 3-10 kV accelerating voltage, 2 nA spot size, and 4 mm working distance.

3.6 Electrical Characterization

Fabricated pellets were polished under a fume hood using 320, 600, 800, and 1200 grit SiC sandpaper. The pellet was then electroded with 100 nm Pt on each side using a Quorum Q150R Sputter Coater [24]. Electrical impedance was performed in box furnaces using a ModuLab XM MTS impedance spectrometer. 12.5°C intervals were selected with a starting temperature of 125°C and a final temperature of 75°C. A 2°C tolerance and 420 second hold time using were selected using a DD9010 temperature controller. The software Z-view was used for EIS analysis.

Chapter 4 Composite Fabrication Results and Discussion

Figure 4.1 Relative Density and % Contents by Weight and Volume of Tested Polyimide Dispersion Methodologies

Method	Wt% RTM	Vol% RTM	Relative Density (%)
Pure ZnO	0.0	0.0	97.0
Dry Hand	5.0	17.7	85.7
Wet Hand	5.0	17.7	86.5
Cryomill	2.5	9.0	88.8
1-step polysol	1.6	6.7	94.7
2-step polysol	1.2	5.0	85.0

Figure 4.2 Examples of Fabricated Composite Pellets

Table 4.1 displays the five methods used for fabricating composite pellets outlined in Chapter 3 along with pure ZnO cold sintering as a control. The two metrics used to measure the quality of a sample are the relative density of the pellets and the dispersion of the polyimide in the microstructure. Polymer dispersion will be qualified via SEM and EDS, and density was quantified via an Archimedes density measurement. 95% density serves as a threshold for a high quality ceramic sample [13]. The effectiveness of the CSP on ZnO is shown via the 97% density obtained on the pure ZnO control. Most fabrication methods tested yielded a sub-optimal relative density in the range of 85-89%. The 1-step polysol method was shown to be inconsistent across

multiple fabricated pellets but yielded up to 94.7% density. Given the sub-optimal density results of the other fabrication methods, 1-step polysol was identified to be the only candidate viable for further analysis.

Figure 4.3 EDS of ZnO-Polyimide Composite Fabricated via the 1-Step Polysol Method

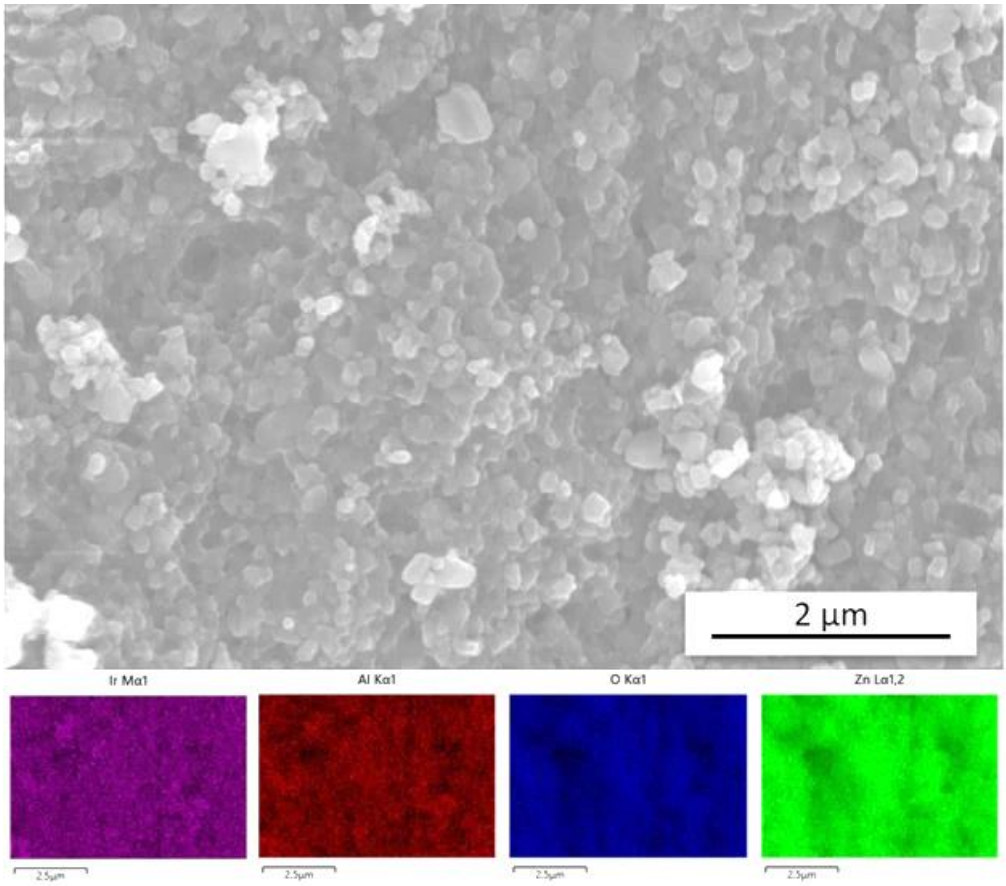

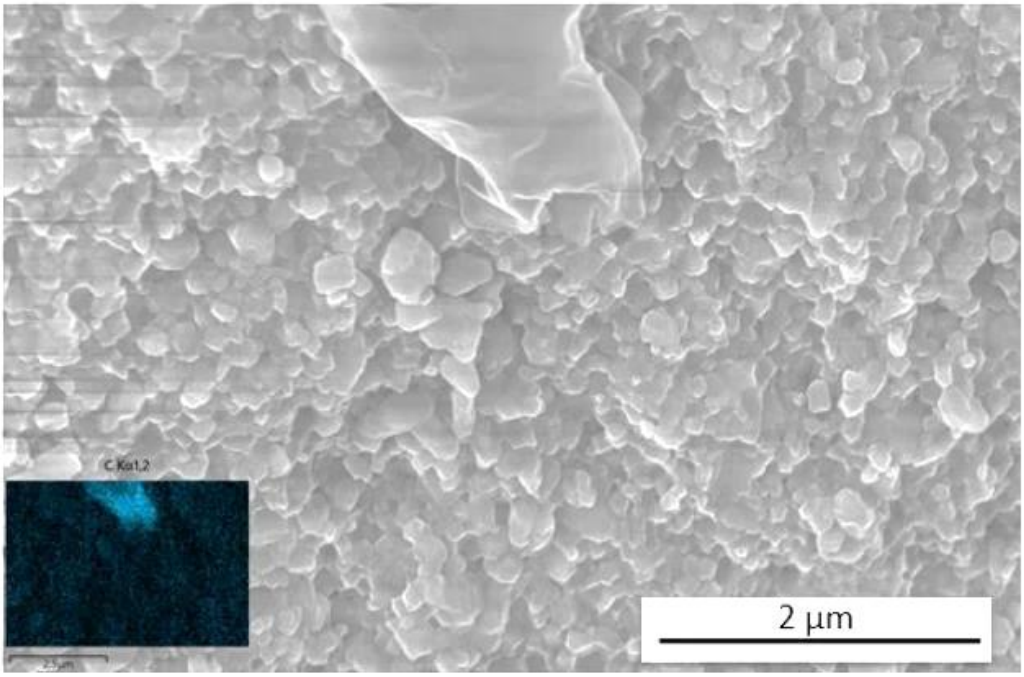

The SEM images in Figure 4.2 qualitatively corroborates the high density recorded in Table 4.1. The EDS image shows ZnO regions with an equiaxed grain morphology consistent with a well sintered ceramic. EDS also revealed unexpected Al content which may be a contaminant but did not have an impact on ceramic sintering. Smooth amorphous phases are present throughout the structure which were confirmed to be aggregated polymer via EDS data showing the polymer's C content. As shown in the idealized composite structure, polyimide was hypothesized to homogenously disperse in the grain boundaries of the ceramic. Some dispersion may be present as seen by C scattering on the EDS image (Figure 4.2), but an SEM image with a wider field of view (Figure 4.3) demonstrates that polymer dispersion was not homogenous, and the polyimide tended to aggregate on top of rather in between the ceramic grains. It should be noted that "on top of the ceramic grains" does not necessarily refer to the surface of the pellet. The polymer was still inside of the pellet, it just likely defined the failure path when the pellet was broken for SEM

analysis. This led to its appearance overlaying the ceramic. Figure 4.4 demonstrates a few grains of ZnO integrated into the polymer, but integration of the two material phases was uncommon.

Figure 4.4 SEM of ZnO-Polyimide Composite Fabricated via the 1-Step Polysol Method

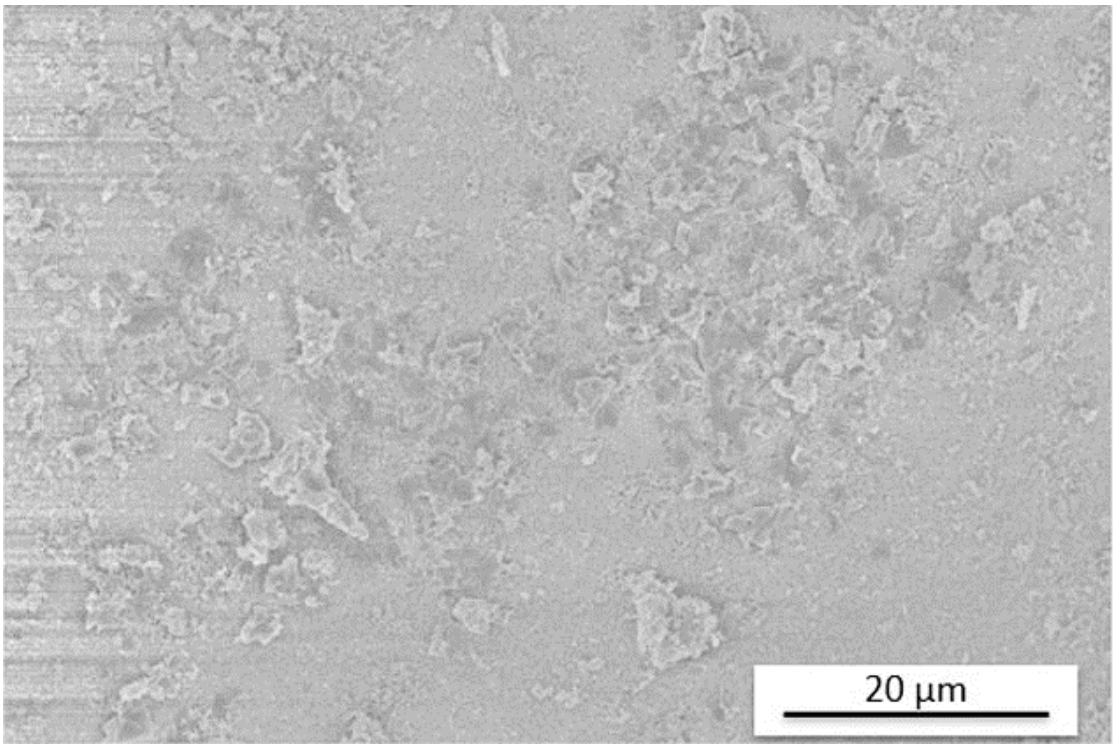

Figure 4.5 SEM Demonstrating Morphology of ZnO Grains in ZnO-Polyimide Composite Fabricated via the 1-Step Polysol Method

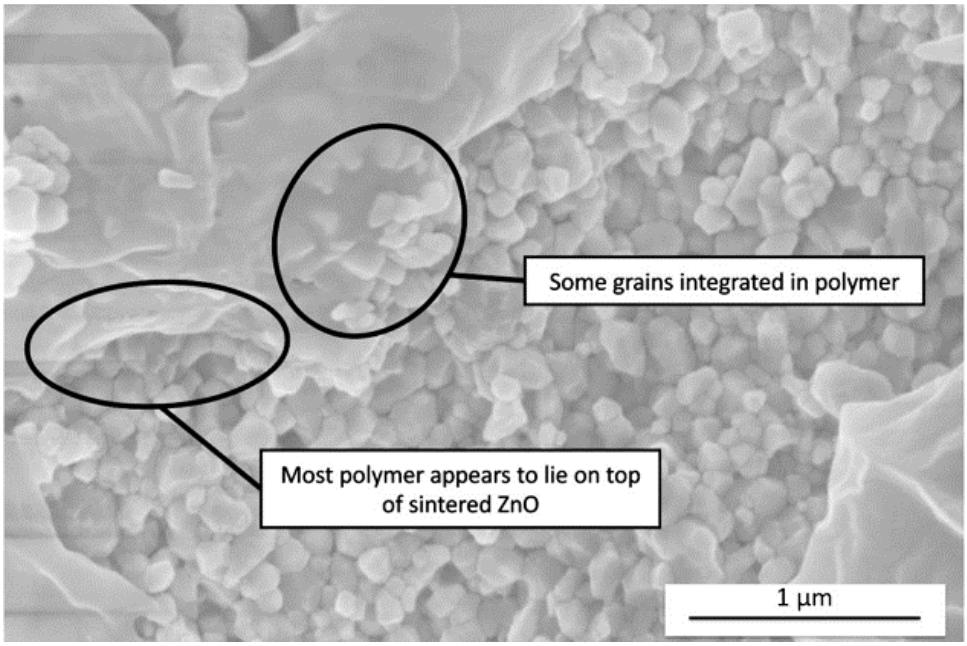

One reason for poor dispersion could be that polyimide does not wet ZnO well. This was qualitatively assessed by melting polyimide on a pure ZnO surface and aluminum foil control (Figure 4.5). The polyimide was found to wet ZnO equivalently if not better than the aluminum foil control, eliminating surface wetting as a limiting factor in polyimide dispersion.

Figure 4.6 Polyimide Wetting on ZnO and Aluminum Foil Surface

In contrast to the 1-step polysol sample, Figure 4.6 displays the microstructure of the cryomilled pellet. There are similar aggregations of polymer, but with a greater degree of incorporation in the ceramic microstructure. SEM also revealed mechanical failure in the form of cracking which the 1-step polysol pellet did not have. The porosity from this cracking likely yielded the sub-par relative density. So though the cryomilled sample displayed marginally better polyimide microstructural integration, it has a trade-off with the greater degree of porosity.

Figure 4.7 SEM of ZnO-Polyimide Composite Fabricated via the Cryomilling Method

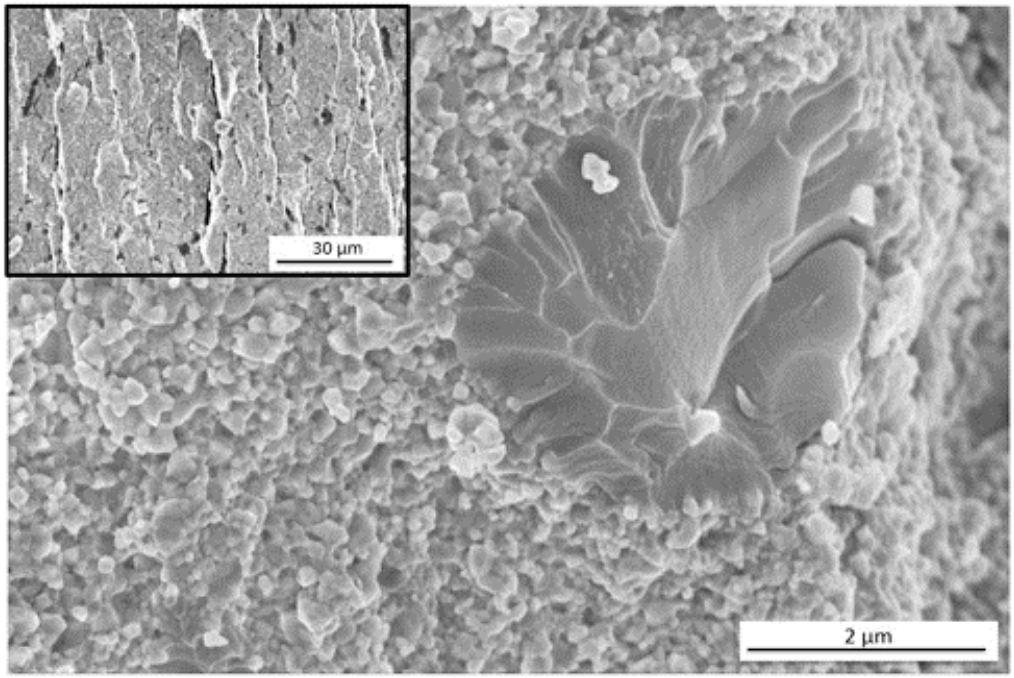

Chapter 5 Internal Polyimide Crosslinking Results and Discussion

Polyimide crosslinking was confirmed externally prior to internal crosslinking of the fabricated pellet. After polyimide crosslinked at 380°C, the polyimide darked in color and significantly increased in hardness. These physical changes served as an indication that a chemical change took place.

Figure 5.1 demonstrates FTIR performed to corroborate this chemical change through the comparison of crosslinked and uncrosslinked polyimide. The disappearance of the 2200 cm^{-1} peak demonstrates the removal of a triple bond between two C atoms [25]. Such a structure is present in the PEPA endcap shown in Figure 5.2. The splitting of this triple bond could participate in the formation of C single bonds between adjacent PEPA groups in different polyimide chains [26]. The remaining peaks that were observed to disappear point to a mechanism involving the aromatic benzene groups in the polyimide. The 1613 and 1425 cm^{-1} peaks correspond to the vibration of benzene C bonds, while the 846, 758, and 574 cm^{-1} peaks suggest the removal of the C and H bond on these benzene groups [25]. In some polyimides the removal of a functional group attached to a benzene can lead to the formation of benzylic free radicals (Figure 5.2), which can form C crosslinks to adjacent polyimide chains [27]. This mechanism may be occurring through deprotonation in the RTM370 polyimide. These proposed mechanisms confirms that a structural change takes place at 380°C.

Figure 5.1 FTIR of RTM370 Polyimide Before and After Crosslinking

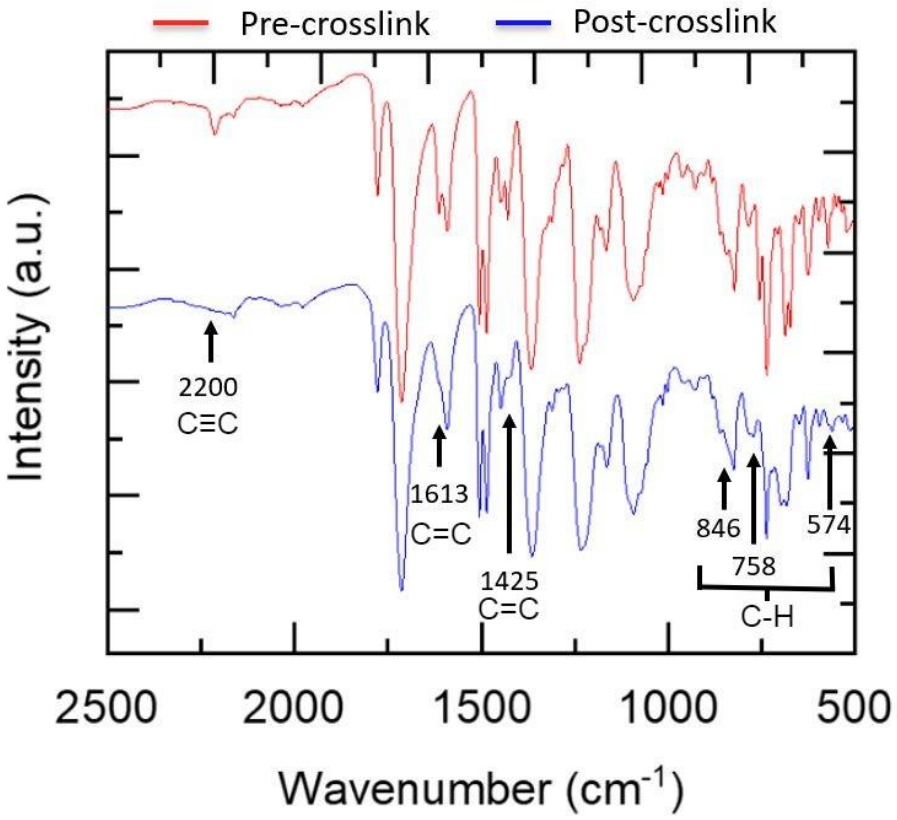

Figure 5.2 Proposed Mechanisms for RTM370 Polyimide Crosslinking

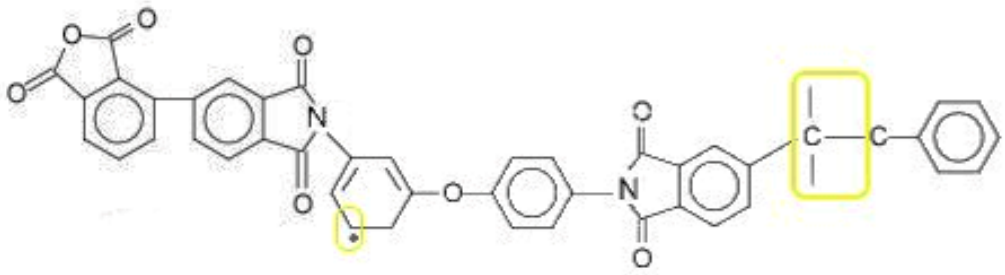

Figure 5.3 1-Step Polysol Composite Pellet Before and After Crosslinking

Figure 5.3 demonstrates the composite pellet after 380°C heat treatment as performed on the externally crosslinked polyimide. The pellet darkened significantly, consistent with the color change observed in polyimide crosslinking.

Figure 5.4 Electrical Impedance of ZnO-Polyimide

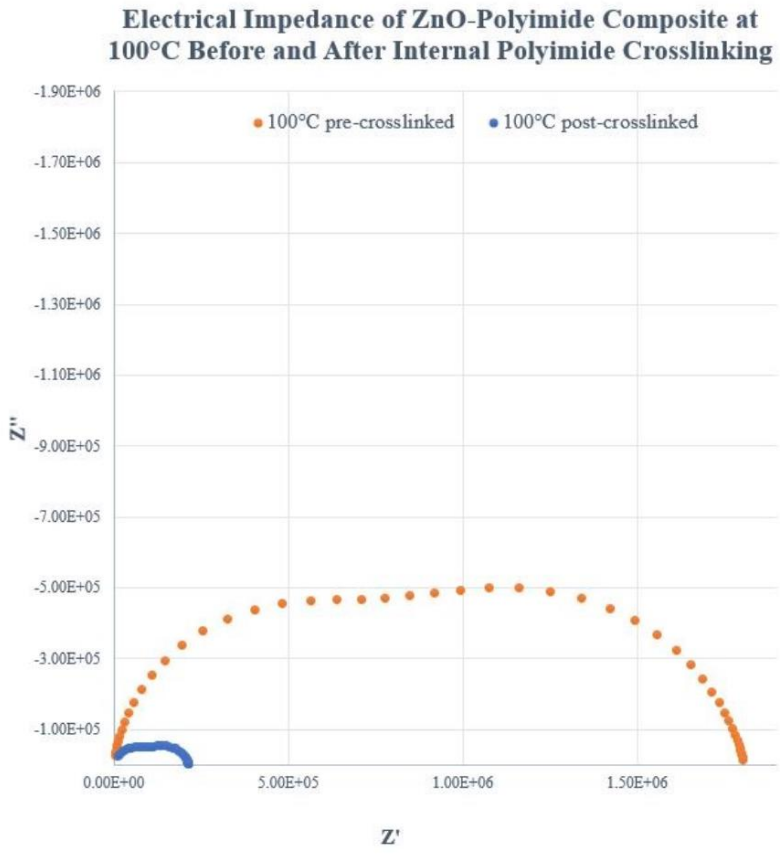

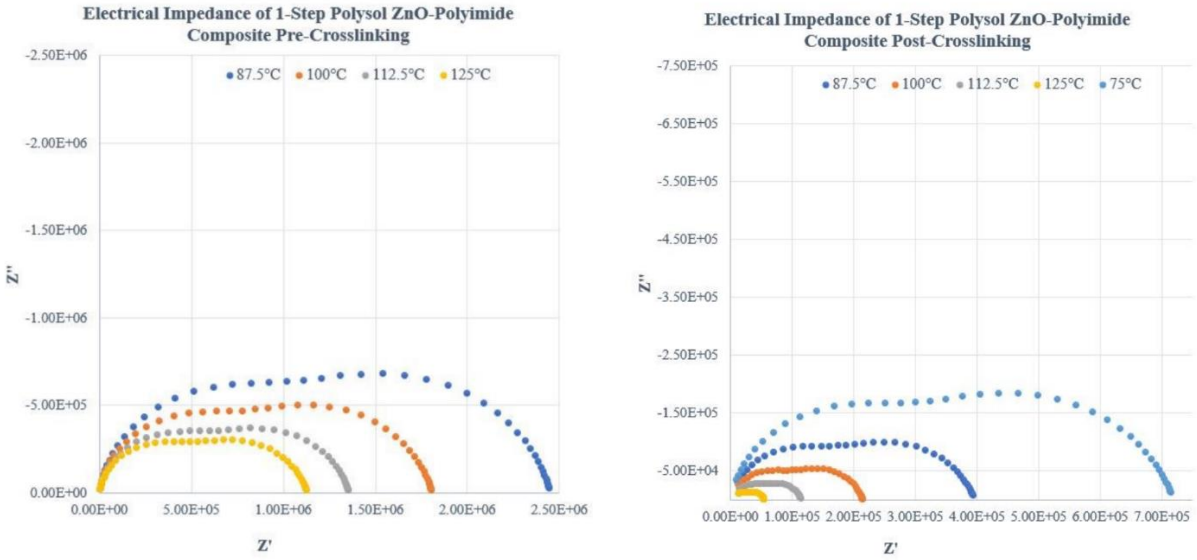

Figure 5.5 Impedance Spectroscopy of Pure ZnO and ZnO-Polyimide Composite

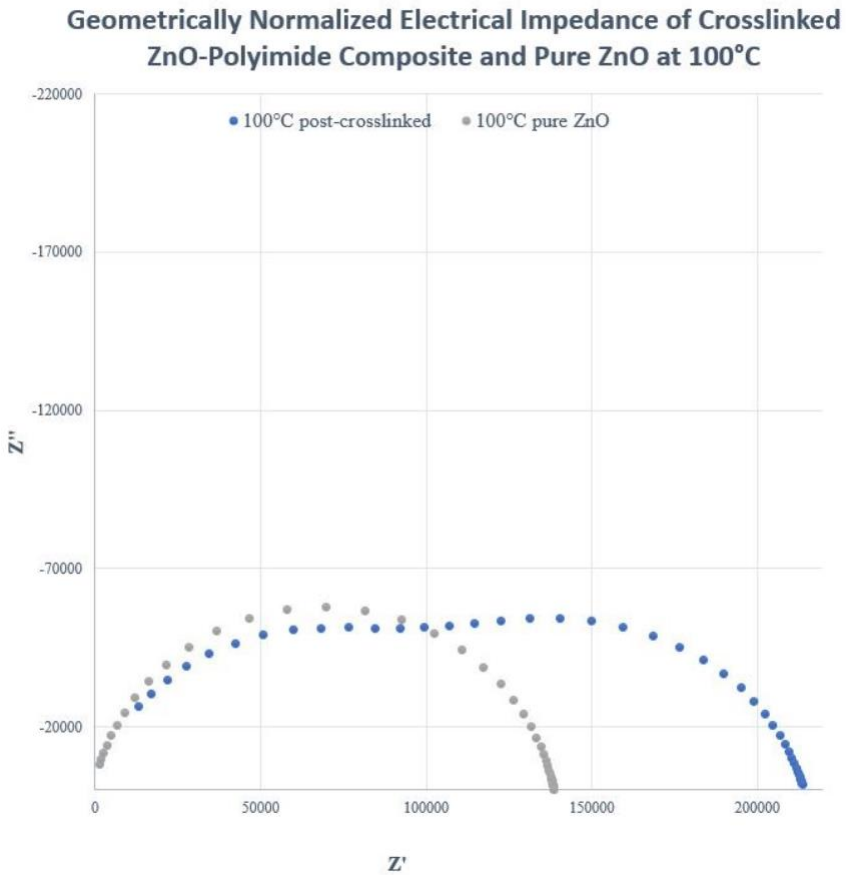

Figure 5.4 displays the impedance spectroscopy for the composite pellet before and after crosslinking. The shape of the semicircle indicates two responses, which is consistent with the expectation of a ZnO and polyimide response. Figure 5.5 geometrically normalizes a pure ZnO pellet to the fabricated composite. The first response of the composite is consistent with the ZnO response. It was shown that resistivity, but not the shape of the response, decreases as a function of temperature. When comparing pre- and post-crosslinking impedance at the same temperature, it is seen that the pre-crosslinked composite has a resistivity of $1.78 \times 10^6\ \Omega \cdot m$ while the crosslinked composite has a resistivity one order of magnitude less at $2.13 \times 10^5\ \Omega \cdot m$. This is opposite the expectation that polymer crosslinking would impede electron conduction between grains and result in a higher resistivity. Table 1 shows the conductivity values of pure ZnO, and the polyimide ZnO composite before and after crosslinking. The trends in resistivity are corroborated, and converse to the stated hypothesis, the conductivity of the composite increased post-crosslinking.

One proposed reason for this observed trend could do with the polyimide crosslinking mechanism. As discussed from the FTIR results in Figure 5.1 and 5.2, deprotonation on the benzene groups of the polyimide results in the formation of benzylic free radicals. If full crosslinking inside of the composite was not achieved, benzylic free radicals may persist in the polyimide structure. Free radicals are atoms with open valence spots and provide a path for electrical conduction through the polyimide. This structural feature therefore could account for the increased conductivity post-crosslinking.

Table 5.1 Conductivity [S/m] of Pure ZnO and ZnO-Polyimide Composite Before and After Crosslinking as a Function of Time

T [°C]	Pure ZnO	Pre-Crosslinked	Post-Crosslinked
75.0	9.01×10^{-7}	-	1.06×10^{-7}
87.5	-	3.13×10^{-8}	1.92×10^{-7}
100.0	1.28×10^{-6}	4.23×10^{-8}	3.53×10^{-7}
112.5	-	5.61×10^{-8}	6.60×10^{-7}
125.0	-	6.78×10^{-8}	1.38×10^{-6}

Figure 5.6 Tan Delta of ZnO-Polyimide Composite as a Function of Frequency

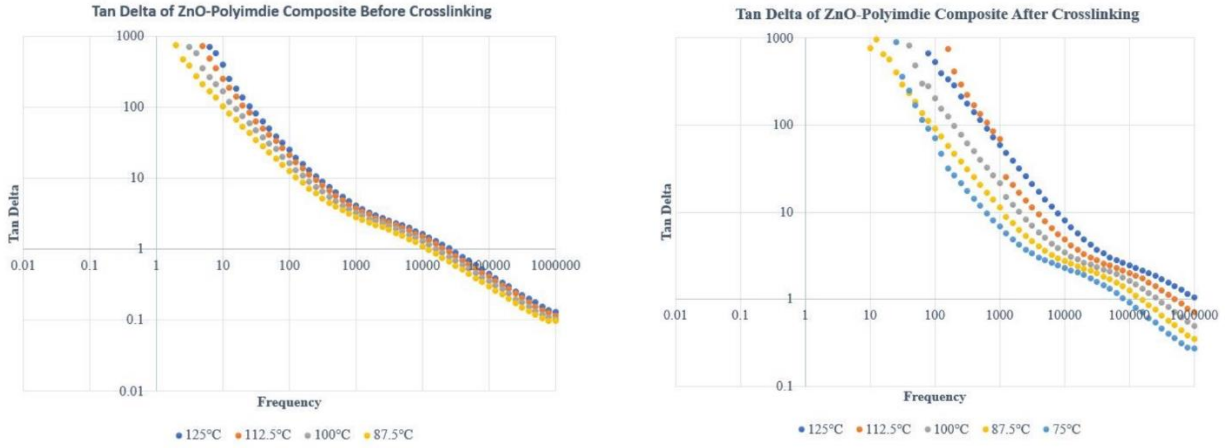

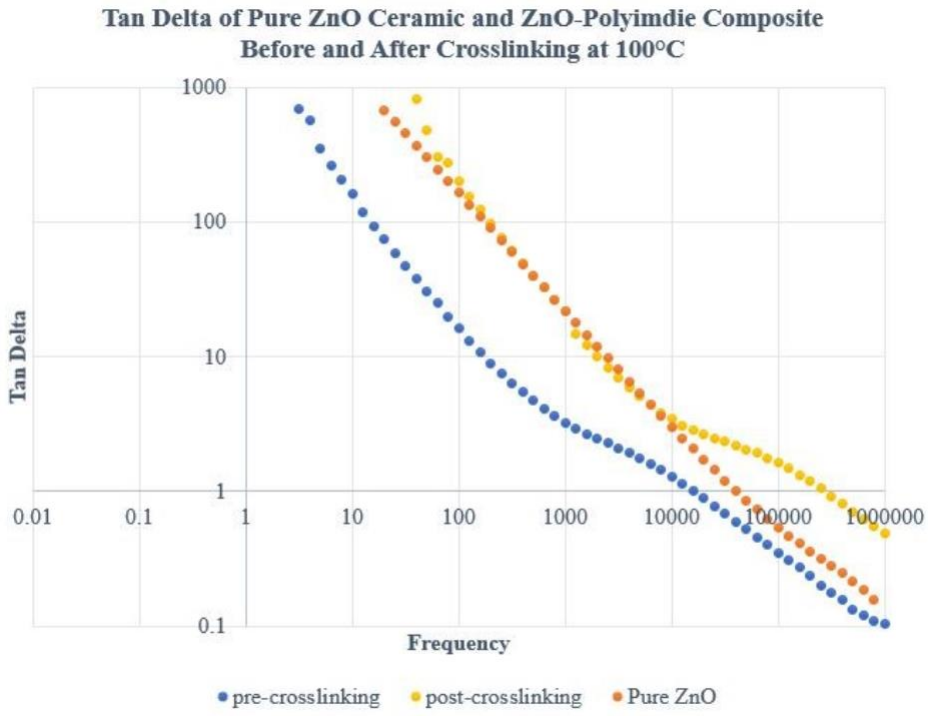

Figure 5.5 displays the tan delta as a function of frequency for the composite pellet before and after crosslinking. Tan delta is a measurement of the loss associated with electron conduction in the impedance spectroscopy measurement where tan delta = ε”/ ε’. Significant loss could indicate error associated with the impedance measurement. A relatively low loss system is expected to have a tan delta of 1 at approximately 1,000 Hz. The high loss of the pure ZnO is an indication that residual organics existed within the structure such as water. The introduction of polyimide before crosslinking lowered the tan delta while crosslinking raised the loss to above that of pure ZnO. The suppressed loss before crosslinking suggests that the polyimide was impeding electron conduction, while the increased loss from crosslinking suggests increased conduction. These trends are corroborated by the measured conduction in Table 5.1. Tan delta varied with temperature more after crosslinking, which is an indication of different activation

energies for electron conduction. This is confirmed and explored further in figure 5.7. While the pure ZnO response is a straight line, the composite tan deltas also indicate a clear second response at higher frequencies, where measurement at the grain boundary level occurs. The higher loss at the grain boundary is evidence of the polyimide existing there. Below approximately 10,000 Hz the tan delta of the composite after crosslinking matches that of pure ZnO, indicating that the long range conduction response matches that of pure ZnO.

Figure 5.7 Activation Energy of Conduction for Pure ZnO and ZnO-Polyimide Composite Before and After Crosslinking

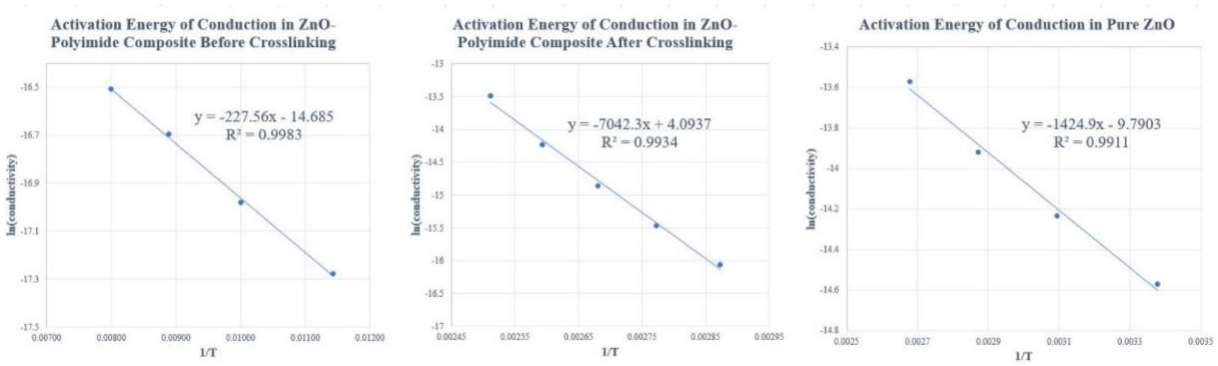

Activation energy plots show that pure ZnO has an activation energy of 0.12 eV. The introduction of polymer, both before and after crosslinking, increased the activation energy of conduction. This is consistent with the expectation that polyimide in the ceramic grain boundaries would resist electron conduction between grains. Before crosslinking, the activation energy was 0.26 eV and after crosslinking it was found to be 0.61 eV. The y-intercept of the Arrhenius relationship is proportional to several factors including the concentration of charge carriers. Before crosslinking the intercept was -14.69, while after crosslinking it was 4.09 indicating that there may be a significant increase in charge carrier concentration. While the

increase in activation error is inconsistent with the results found that conduction increased with crosslinking, a greater amount of charge carriers serves as a possible explanation for the observed trend. Crosslinking could increase charge carrier concentration through the creation of benzylic free radicals as presented in the proposed polyimide crosslinking mechanism. These trends warrant further investigation, particularly in the confirmation of free radicals as the charge carrier post-crosslinking.

Figure 5.8 shows an SEM image taken after polymer crosslinking. EDS reveals some Al contamination and the expected Zn and O matrix associated with the ceramic phase as shown before in pre-crosslinking images. Unlike before crosslinking, EDS suggests there is a much higher dispersion of C than previously found. This was a consistent trend found throughout the bulk structure of the composite.

Figure 5.8 EDS of ZnO-Polyimide Composite Fabricated via the 1-Step Polysol Method After Crosslinking

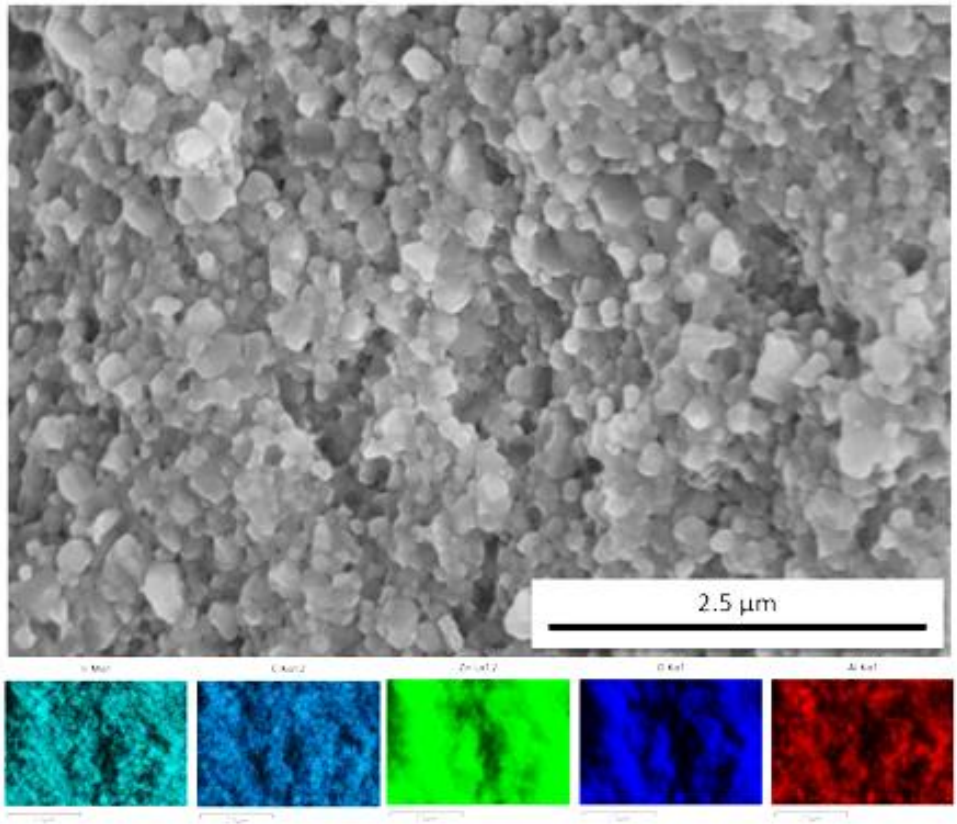

Another hypothesis for the increase in conductivity after crosslinking is that polyimide degradation into smaller constituents or elemental C could conduct electrons well. The acetic acid transient solvent could serve as a chemical degrading agent. FTIR was performed on polyimide exposed to 2 M acetic acid for 24, 48, and 72 hours and no change in absorption peaks, and therefore no degradation, was found (Figure 5.9) [25]. The nearly 95% dense ceramic structure would suggest that there is no physical volume for polyimide dispersion or movement. As a result, the greater dispersion of polyimide after crosslinking is either the result of an error with the preformed EDS or the mechanism is not clearly understood.

Figure 5.9 Polyimide FTIR with Key Structural Groups Labeled after 2 M Acetic Acid Exposure for 24, 48, and 72 Hours

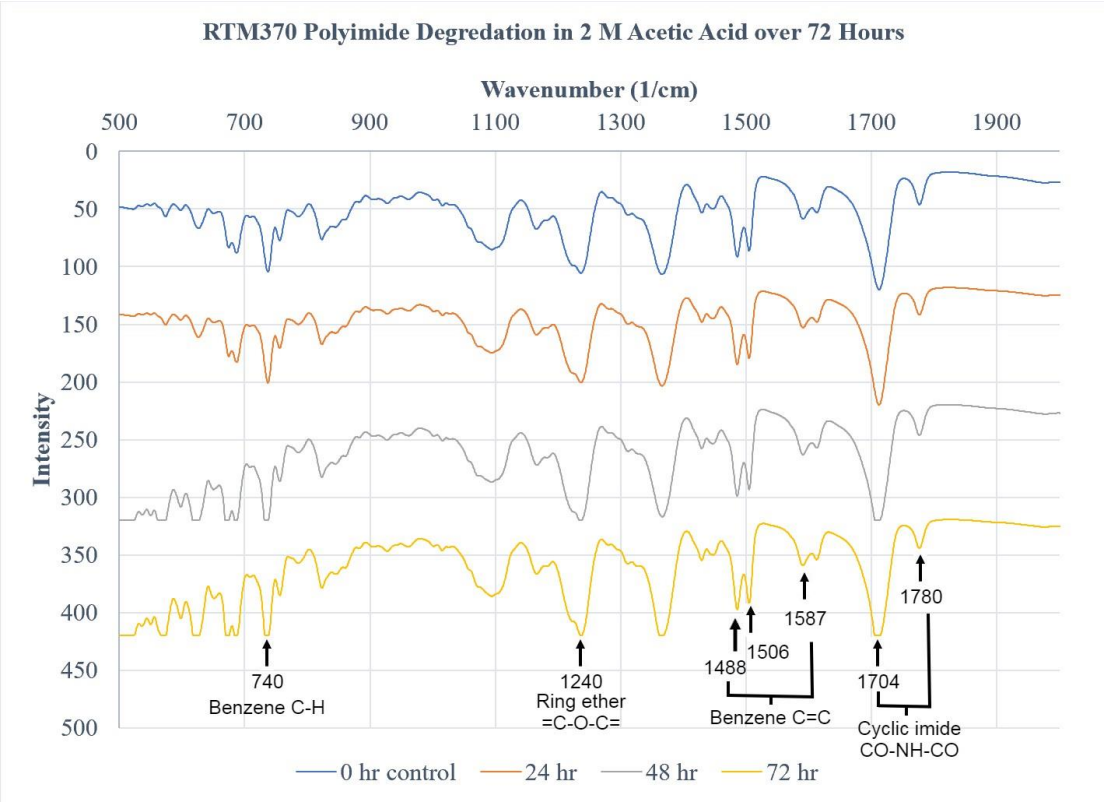

Chapter 6

Conclusion and Future Work

This thesis outlined a methodology for the creation of a dense ZnO-polyimide composite via the cold sintering method. Five methods of polyimide dispersion in ZnO were explored and the 1-step polyimide method was identified as the best procedure for obtaining dense composites. SEM and EDS analysis revealed that while a dense ceramic structure was obtained, ideal homogenous polyimide dispersion was not. FTIR analysis of polyimide after 380°C heat treatment reveled a crosslinking mechanism resulting from the splitting of an alkyne group and the formation of a benzylic free radical via deprotonation. The main objective of chemically altering a polymer phase inside of a composite was successfully achieved. Converse to expectations, impedance spectroscopy revealed that heat treating the composite at 380°C increased the conductivity by an order of magnitude. Both composites had a lower conductivity than pure ZnO, but crosslinking significantly increased the concentration of charge carriers. It was hypothesized that this increase in charge carrier concentration resulted from the proposed benzylic free radical mechanism during polyimide crosslinking.

While this ZnO-polyimide system successfully served as a composite proof of concept demonstrating internally tunable properties as a function of heat post-cold sintering, there is much about the material that is still not well understood. Further investigation is warranted in the polyimide dispersion methodology. Ideal homogenous polyimide dispersion was not successfully achieved before cold sintering, demanding modification to the 1-step polysol method detailed in this thesis. SEM and EDS images post-crosslinking also revealed an appreciable increase in polyimide dispersion after crosslinking which, given the limited free volume as a result of the nearly 95% dense ceramic structure, is not well understood. Further investigation is also needed

in understanding the cause of the change in electrical resistivity found via impedance spectroscopy. This investigation performed FTIR analysis on externally crosslinked polyimide, but FTIR analysis also should be performed directly on the sample to verify the crosslinking of internal polyimide. Thermal characterization methods like differential scanning calorimetry (DSC) could also be used to identify phase changes. Impedance spectroscopy performed on systems with known benzylic free radicals could be used to help confirm the hypothesized free radical charge carrier mechanism for electrical conduction in the crosslinked composite. Understanding how microstructurally the observed electrical trends occurred could be useful in adapting internally tunable composite systems for use in real applications in the future like varistors.

References

1. Guo, J., Berbano, S.S., Guo, H., Baker, A.L., Lanagan, M.T. and Randall, C.A. (2016), Cold Sintering Process of Composites: Bridging the Processing Temperature Gap of Ceramic and Polymer Materials. Adv. Funct. Mater., 26: 7115-7121. https://doi.org/10.1002/adfm.201602489
2. Ponnamma, Deepalekshmi, et al. "Synthesis, optimization and applications of ZnO/polymer nanocomposites." *Materials Science and Engineering: C* 98 (2019): 1210-1240.
3. Callister, W.D., & Rethwisch, D.G. (2014). *Materials Science and Engineering: and Introduction* (9E ed.). Wiley.
4. Ednie-Brown, P. (2013), bioMASON and the Speculative Engagements of Biotechnical Architecture. Archit Design, 83: 84-91. https://doi.org/10.1002/ad.1529
5. *Making concrete change: Innovation in low-carbon cement and concrete*. (2018, June 13). Chatham House – International Affairs Think Tank. https://www.chathamhouse.org/2018/06/making-concrete-change-innovation-low-carbon-cement-and-concrete
6. *Sedghi, Arman & Noori, Nastaran. (2011). Comparison of electrical properties of zinc oxide varistors manufactured from micro and nano ZnO powder. Journal of Ceramic Processing Research. 12. 752-755.* Small, C. E., Chen, S., Subbiah, J., Amb, C. M., Tsang, S.-W., Lai, T.-H., Reynolds, J. R., & So, F. (2012). High-efficiency inverted dithienogermole–thienopyrrolodione-based polymer solar cells. *Nature Photonics*, *6*(2), 115–120. https://doi.org/10.1038/nphoton.2011.317

7. Small, Cephas E., et al. "High-efficiency inverted dithienogermole–thienopyrrolodione-based polymer solar cells." *Nature Photonics* 6.2 (2012): 115-120.
8. Gomez, E. D., Randall, C. A., Arguelles, A., & Sun, H. (n.d.). *Fmsg: Eco: integration and recycling of high quality ceramics and composites enabled by scalable cold sintering manufacturing*. Penn State. Retrieved March 8, 2022, from https://pennstate.pure.elsevier.com/en/projects/fmsg-eco-integration-and-recycling-of-high-quality-ceramics-and-c
9. Chuang, K., Criss, J. M., Mintz, E., Scheiman, D., Nguyen, B., & McCorkle, L. (2007). Low-melt viscosity polyimide resins for resin transfer molding (Rtm) ii. *NASA*. https://www.semanticscholar.org/paper/LOW-MELT-VISCOSITY-POLYIMIDE-RESINS-FOR-RESIN-(RTM)-Chuang-Criss/3351f25519dcd9465058391051c071fff3effb6b
10. Supatutkul, C., et al. “Electronic Properties of Two-Dimensional Zinc Oxide in Hexagonal, (4,4)-Tetragonal, and (4,8)-Tetragonal Structures by Using Hybrid Functional Calculation.” Journal of Physics: Conference Series, vol. 901, Sept. 2017, p. 012172. DOI.org (Crossref), doi:10.1088/1742-6596/901/1/012172.
11. Hüpkes, Jürgen, et al. “Chemical Etching of Zinc Oxide for Thin-Film Silicon Solar Cells.” ChemPhysChem, vol. 13, no. 1, 2012, pp. 66–73. Wiley Online Library, doi:https://doi.org/10.1002/cphc.201100738.
12. Callahan, M. J., et al. “Growth Mechanisms and Properties of Hydrothermal ZnO.” Zinc Oxide Materials for Electronic and Optoelectronic Device Applications, John Wiley & Sons, Ltd, 2011, pp. 189–220. Wiley Online Library, doi:10.1002/9781119991038.ch8.

13. Guo, Jing, et al. "Cold sintering: a paradigm shift for processing and integration of ceramics." *Angewandte Chemie* 128.38 (2016): 11629-11633.

14. Sengul, Mert Y., et al. “ReaxFF Molecular Dynamics Study on the Influence of Temperature on Adsorption, Desorption, and Decomposition at the Acetic Acid/Water/ZnO($10\bar{1}0$) Interface Enabling Cold Sintering.” ACS Applied Materials & Interfaces, vol. 10, no. 43, Oct. 2018, pp. 37717–24. ACS Publications, doi:10.1021/acsami.8b13630.

15. *Zno etching in acetic acid mechanism animation psu matse 400 honors option*. (n.d.). Retrieved March 8, 2022, from https://www.youtube.com/watch?v=n0Y33Jmlmf0

16. Bonanos, N., et al. "Applications of impedance spectroscopy." *Impedance spectroscopy: Theory, experiment, and applications* (2018): 175-478.

17. Sahay, P. & Tewari, S. & Nath, Rajarshi & Shamsuddin, M.. (2008). Studies on ac response of zinc oxide pellets. *Journal of Materials Science*. 43. 4534-4540. 10.1007/s10853-008-2642-x.

18. Gerhardt, R. (1994). Impedance and dielectric spectroscopy revisited: Distinguishing localized relaxation from long-range conductivity. *Journal of Physics and Chemistry of Solids*, *55*(12), 1491–1506. https://doi.org/10.1016/0022-3697(94)90575-4

19. Dutta, A. (2017). Chapter 4—Fourier transform infrared spectroscopy. In S. Thomas, R. Thomas, A. K. Zachariah, & R. K. Mishra (Eds.), *Spectroscopic Methods for Nanomaterials Characterization* (pp. 73–93). Elsevier. https://doi.org/10.1016/B978-0-323-46140-5.00004-2

20. *Sem/eds analysis | RTI laboratories*. (2016, February 22). https://rtilab.com/techniques/sem-eds-analysis/

21. Levinson, Lionel & Philipp, Herbert. (1986). ZINC OXIDE VARISTORS - A REVIEW.. American Ceramic Society Bulletin. 65. 639-646.

22. *Milling and mixing in the materials characterization lab*. (n.d.). Retrieved March 8, 2022, from https://www.mri.psu.edu/materials-characterization-lab/sample-prep/milling-and-mixing

23. *Fourier transform infrared spectroscopy(FTIR)*. (n.d.). Retrieved March 8, 2022, from https://www.mri.psu.edu/materials-characterization-lab/characterization-techniques/fourier-transform-infrared-spectroscopy

24. *Sputtering sample prep at the materials characterization lab*. (n.d.). Retrieved March 8, 2022, from http://www.mri.psu.edu/materials-characterization-lab/sample-prep/sputtering

25. Socrates, George. *Infrared and Raman characteristic group frequencies: tables and charts*. John Wiley & Sons, 2004.

26. Wang, T., Yang, Y., Song, N., Zhu, S., Yao, H., Zhang, Y., & Guan, S. (2021). Thermal crosslinking polymerization of aromatic alkynyl monomers to microporous polyimides in diphenyl sulfone. *Microporous and Mesoporous Materials*, *328*, 111447. https://doi.org/10.1016/j.micromeso.2021.111447

27. Xu, S., Ren, X., Zhao, N., Wu, L., Zhang, Z., Fan, Y., & Li, N. (2021). Self-crosslinking of bromomethylated 6FDA-DAM polyimide for gas separations. *Journal of Membrane Science*, *636*, 119534. https://doi.org/10.1016/j.memsci.2021.119534

ACADEMIC VITA

Adam Vetser

EDUCATION:

The Pennsylvania State University (University Park, PA) *August 2018 - May 2023 (anticipated)*

- BS and MS in Material Science Engineering through integrated undergraduate program
- Schreyer Honors College

WORK EXPERIENCE:

GE Aviation Engineering Materials Systems Technical Intern (Evendale, OH) *Summer 2021*

- Developed technical skills in the fields of jet engine tribology, oxidation, and corrosion through 12-week co-op in the Coatings, Surfaces, and Environmental Behavior group.
- Contributed to **over 15** engine programs including:
    - Office of Naval Research program studying diffusion between metals and novel ceramic matrix composites in high temperature engine environments.
    - Thermal barrier coating spallation studies for the GENX engine.
    - Clean and peen repair program characterizing corrosive pitting on field hardware.

GE Aviation Virtual Intern Academy *Summer 2020*

- Trained in jet engine basics and fundamentals of lean and six sigma.
- Collaboratively completed New Product Integration (NPI) simulation.
- Distinguished myself by earning "exceeded expectations" evaluation and placing **4th** in the engagement competition and social impact team project.

Materials Research Institute Undergraduate Thesis Research *Fall 2020-current*

- Researcher in Dr. Clive Randall's group pursuing senior thesis in cold sintering of zinc oxide/polyimide composite materials.

Undergraduate Research in Polymers *Fall 2019-Fall 2020*

- Researcher in Dr. Michael Hickner's polymers lab researching dual extrusion Silicone and Nylon 3D printing.

INTERPERSONAL SKILLS:

World in Conversation Facilitator *Fall 2021*

- In training to develop communication skills for facilitating group discussions on social issues as a part of the Penn State World in Conversation program.

Public Speaking Mentor *Spring 2020-current*

- Perfected and taught communication, writing, and visual aid design skills.

Teaching Assistant Math 140G/141G *Fall 2019-current*

- Assist first year students with Earth and Mineral Science-focused calculus math concepts through one on one and group tutoring.
- Improved ability to communicate analytical concepts.

VOLUNTEER EXPERIENCE:

Generation Impact Social Hackathon Competition *Summer 2020*

- Developed hackathon program pitch in a team of five to address housing sustainability through GE's internal social impact organization.

Homework Helpers Coordinator *September 2014 - June 2018*

- Led free tutoring service by directing program activities, recruiting tutors, and tutoring students.